ROYAL SOCIETY
OF CHEMISTRY

## PAPER

CrossMark
click for updates

# Exchange coupling in an electrodeposited magnetic bilayer of Prussian blue analogues†

Juan P. Prieto-Ruiz, Francisco M. Romero, Helena Prima-García* and Eugenio Coronado*

Bilayers of Prussian blue analogues (PBA) constituted of hard and soft magnets have been fabricated by means of electrochemical deposition. This method affords a good contact between two PBA thin films of nanometer thickness. Complete characterization of the resulting system has been performed, which has allowed the determination of the preservation of the chemical identity of both materials during the electrodeposition and the establishment of a clear interface between them. The magnetic behavior of the bilayer can be explained in terms of an exchange-spring magnet.

## 1. Introduction

The study of exchange coupling in nanostructured magnetic systems has drawn major attention in the past few decades.[1–10] A remarkable example is the combination of ferromagnetic (FM) and antiferromagnetic (AFM) materials giving rise to the so-called exchange bias interaction,[2–6] especially interesting due to the fundamental role of this effect in the development of spin valves and tunneling devices.[3]

In this context, the exchange-spring magnets (ESMs)[7–10] are also systems of major interest, being classically composed of a two-phase distribution of hard- and soft-magnetic grains.[7] In the first place, the interest of ESMs relies on the fact that they are able to provide a model system which can complement the understanding of the exchange-bias problem.[11] Additionally, ESMs are promising candidates as permanent magnets due to their large energy products $(BH)_{max}$, compared to traditional single-phase materials.[7,12,13] Future applications in this vein include two-phase randomly dispersed nanocomposites[7,13] as well as coupled bilayer films.[8,9] In the latter case, the better control over magnetic and structural parameters, such as thickness or interfacial exchange coupling strength, has promoted their extensive study.[14] So far, the reported studies on this line have been mainly limited to bilayer or multilayer systems composed of inorganic magnetic materials grown epitaxially by expensive evaporation techniques.[8,9,15] Still, some molecule-based materials composed either of hard magnets in direct contact with soft magnets,[16,17] or an anisotropic molecule inside a soft magnetic lattice,[18] have also shown an ESM behavior.

*Instituto de Ciencia Molecular (ICMol), Universitat de València, C/Catedrático José Beltrán 2, 46980-Paterna, Spain. E-mail: helena.prima@uv.es, coronado@uv.es*

Some of these examples have been provided by Prussian blue analogues (PBAs). These coordination polymers with general formula $C_cA_a[B(CN)_6]_b \cdot nH_2O$ (C = alkali cation, A, B = transition metal ions) are molecule-based systems with interesting magnetic properties. Reversible switching of magnetization or magnetic pole inversion[19] mediated by different physical and chemical stimuli (visible light,[20,21] X-rays,[22] pressure,[23,24] and temperature[25]) has been extensively reported. These interesting properties have motivated the application of PBAs for the fabrication of bilayers and heterostructures which may display new properties arising from the interaction between the two components. Along this line, a remarkable example of ESM has been provided by core–shell nanoparticles based on PBA coordination networks.[16,17] In this case a significant increase in the coercive field of the nanoparticles has been found which has been ascribed to an efficient exchange coupling between the core (soft magnet) and the shell (hard magnet) as a result of the good epitaxial growth between the two magnetic phases. Another study concerns the multilayers of magnetic and photomagnetic PBA.[26–28] By combining these materials in a thin film, a photoinduced enhancement of the critical temperature with respect to the isolated photoactive compound has been reported. This situation can be understood based on the direct interfacial coupling of the two lattices in the structure. In the same vein, a heterostructured system with interesting novel photomagnetic properties composed of a PBA and a 3D Hofmann-like spin crossover compound was described recently.[29]

In the present work, a sequential electrochemical approach has been applied for the fabrication of a PBA bilayer formed by a bottom layer of $Cr_{5.5}(CN)_{12} \cdot 11.5H_2O$ (**CrCr**) electrodeposited[30–34] on a gold substrate and a top ultrathin film of $Fe_3[Cr(CN)_6]_2 \cdot 15H_2O$ (**FeCr**) electrodeposited onto the bottom layer.[35,36] It is shown that this heterogeneous magnetic system shows proximity effects, such as exchange bias and exchange-spring magnetism, which are characteristic of magnetic bi(multi)-layers.

# 2. Experimental section

## Synthesis

$K_3[Cr(CN)_6]$, $CrCl_3$ and $FeCl_3$ were purchased from Sigma-Aldrich and used without further purification. The deionized water employed in all the preparation process was obtained from a Millipak Express 20 Millipore system. A sequential electrodeposition approach was employed for the fabrication of the PBA bilayer, as depicted schematically in Fig. 1a. A first electrochemical cell was charged with an aqueous solution (20 mL) containing $K_3[Cr(CN)_6]$ (5 mM) and $CrCl_3$ (7.5 mM). By following the reported procedure[30] electrodeposited films of **CrCr** were grown at a fixed potential ($E = -0.88$ V vs. Ag/AgCl reference electrode) on a substrate of Mylar (dimensions: $5 \times 10$ mm) coated with an evaporated Au layer of 100 nm thickness acting as a working electrode. A Metrohm AUTOLAB potentiostat in the coulometry mode was employed for depositing the films. A Pt electrode was used as a counter electrode. After preparation, **CrCr** films were rinsed with water and subsequently transferred to a second solution containing the precursors for the electrodeposition of the top PBA layer. Employing the same three electrode configuration, a second electrochemical cell was filled with an aqueous solution (20 mL) containing $K_3[Cr(CN)_6]$ (5 mM) and $FeCl_3$ (7.5 mM). By reducing the electrolytic solution at a fixed potential of $E = -0.5$ V, thin films of **FeCr** were synthesized[35] directly on top of the **CrCr** layer. The choice of the order employed for the sequential electrodeposition is based on the relative value of the reduction potentials. The prior **CrCr** electrodeposition at $E = -0.88$ V guarantees that the **FeCr** film synthesized on top at $E = -0.5$ V does not produce any chemical change in this bottom layer. This point was confirmed by performing cyclic voltammetry (CV) in a **CrCr** film of 175 nm thickness. With this aim, the film was electrodeposited in the first electrolytic solution. Subsequently, it was transferred to a 0.2 M KCl solution, where a CV study was performed at a scan rate of 20 mV s$^{-1}$ (Fig. 1b). From the CV curve it was possible to observe a quasi-reversible reduction wave scan centered at approximately $-0.85$ V vs. Ag/AgCl, corresponding to the reduction

of the hexacyanochromate anion.[34] Thus, the electroactive region (A) of **CrCr** is located outside the potential window (B) at which the electrodeposition of the **FeCr** layer is performed ($E = -0.5$ V).

## Characterization techniques

An Ambios Technology XP-1 profilometer placed on a vibration isolation table was used for determining the thicknesses of the films. Infrared spectra of the electrodeposited films of **CrCr** and **FeCr** were recorded on a Nicolet 5700 FT-IR spectrometer using a Veemax II specular reflectance accessory. Inductively coupled plasma mass spectrometry (ICP-MS) characterization was performed on an ICP-MS Agilent 7700x including HMI (high matrix introduction) and He mode ORS as standard. The agilent octopole reaction system (ORS) introduces a mode of cell/reaction cell (CRC) – He collision mode – that allows the removal of all polyatomic species based on their size rather than their relative reactivity with the reaction gas. By employing this mode, it is possible to remove interferences (plasma-based and matrix-based) from the ICP-MS measurements, which allows us to combine multi-element screening or Semiquant analysis with an effective interference removal. Standard solutions were purchased from Merck (Certipur® Reference Material ICP Multi Element Standard Solution IV). The morphological characterization of the electrodeposited films was performed by means of a Nanoscope Multimode (Veeco) atomic force microscope operated in the tapping mode. RMS roughness and average particle size were analyzed by using WSxM4 4.0 Develop 13.0 software 38, developed by Nanotec Electronics S.L. HRTEM-STEM studies were performed on a Tecnai F30 (FEI Company) operated at 300 kV. The size, morphology and crystalline structure of each of the layers were obtained from the high resolution TEM (HRTEM) images. An EDAX detector and a Tridiem (Gatan) Energy Filter, respectively, in the scanning transmission electron microscopy mode (STEM) were employed in order to get a chemical profile of the fabricated bilayer lamella. Variable-temperature (applied field: 100 Oe) and field-dependent ($T = 2$ K) dc magnetization measurements were carried out on a Quantum Design MPMS SQUID magnetometer. Bilayers of **CrCr** and **FeCr** on Mylar were cut into two pieces and were introduced in the sample holder with the applied magnetic field parallel to their surface.

# 3. Results and discussion

## General characterization of the electrodeposited PBA bilayer

For both materials in the bilayer, an electrodeposition time of 20 seconds was chosen in order to obtain an appropriate film thickness with a sufficient magnetic signal allowing accurate characterization. The preservation of the chemical identity of each layer during the sequential electrodeposition process was proved by FT-IR spectroscopy (Fig. S1, ESI†). From this measurement the presence of **CrCr** is identified from a band located at 2186 cm$^{-1}$ corresponding to the cyanide stretching vibration of the $[Cr^{III}(CN)_6]^{3-}$ anion.[30] The presence of the **FeCr** layer directly electrodeposited on top is evidenced by a shoulder
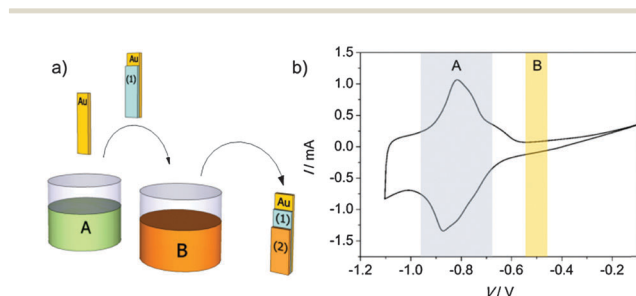


Fig. 1 (a) Scheme of the sequential electrodeposition method used in the preparation of the PBA bilayer, employing a Ag/AgCl (3 M NaCl) reference electrode and a Pt counter electrode. The Au working electrode is introduced in electrolyte A. The first electrodeposition generates the film of **CrCr**. Subsequently the first film is transferred to electrolyte B, where the second layer of **FeCr** is electrodeposited to produce the final bilayer. (b) Cyclic voltammogram of a 175 nm thick film of **CrCr** performed in a 0.2 M KCl solution at 20 mV s$^{-1}$. In blue (A) is indicated the electroactive region of the **CrCr** film and in red (B) the area corresponding to the window of voltage applied for the electrodeposition of **FeCr**.

located at 2165 cm$^{-1}$ corresponding to the cyanide stretching vibration of Cr$^{III}$–C≡N–Fe$^{2+}$ moieties.[35]

The surface morphology of the PBA layers was studied by AFM. The 3D topography images of 25 μm$^2$ scan size, obtained in the tapping mode for each layer composing the bilayer, are shown in Fig. S2 (ESI†). The deposition of the first layer of **CrCr** on the gold electrode after 20 seconds leads to the typical surface morphology reported previously for this kind of PBA.[30,31] Pyramidal grains with an average grain size of 180 nm and surface roughness with an RMS value of 17 nm are observed. This morphology can be related to the epitaxial growth of this electrodeposited PBA on the gold electrode.[37] The electrodeposition dynamics of this molecule-based film consists of a fast initial growth on the gold electrode (nucleation process) with a decrease of the electrodeposition rate as the substrate is covered. Subsequently, the crystallization process takes place leading to the formation of bigger grains as the time of deposition is increased.[30,31] The growing of the second **FeCr** layer for 20 seconds on top of the bottom **CrCr** film generates a grain structure in the surface with an RMS roughness of 26 nm and an average grain size of 190 nm. Isolated grains with sizes ranging between 500 and 600 nm appear in this **FeCr** top layer. In this context, the surface features of the **FeCr** layer are strongly influenced by the direct deposition onto of the **CrCr** film, which presents a lower conductivity than the naked Au working electrode.

A morphological analysis of the system was completed by TEM-STEM characterization (Fig. 2) in order to describe the features of the interface between both materials. These have a major impact on the resulting magnetic coupling between the two PBA systems. From the HR-TEM images of the bilayer, a total thickness of 235 nm was measured. As the elements composing the two layers (Fe and Cr) have a very similar atomic number, $Z$, the determination of the interface by direct contrast was not possible. Nevertheless, profilometry measurements were employed in order to determine the thickness of each layer in the composed structure. Using this technique, a thickness of 175 nm was extracted for a **CrCr** thin film after 20 s deposition time, leading to a value of 60 nm for the **FeCr** layer deposited on top. For overcoming the lack of contrast of HR-TEM images, an element-specific STEM study was performed on the system, obtaining a chemical profile of the materials. In this PBA bilayer, Fe is only present on the top film. Thus, this element was employed for determining the point at which the interface between both materials is located. Fig. 2 shows a representative chemical profile of a large set of measurements obtained by STEM on a lamella of the bilayer. Based on the evolution of the K-line of Fe in the sample, the presence of this element is clearly observed up to 50 nm from the top Pt deposited for the fabrication of the lamella. Subsequently, a progressive decrease is detected along the next 10 nm, point from which the Fe signal vanishes. This value is in agreement with the data extracted from HR-TEM and profilometry for the top **FeCr** layer. In addition, by this characterization a clear interface with an extension of 10 nm is established, with the same order of magnitude as the RMS roughness of the **CrCr** bottom layer. Moreover, an interpenetration of the top PBA film during electrodeposition can be ruled out from these measurements.
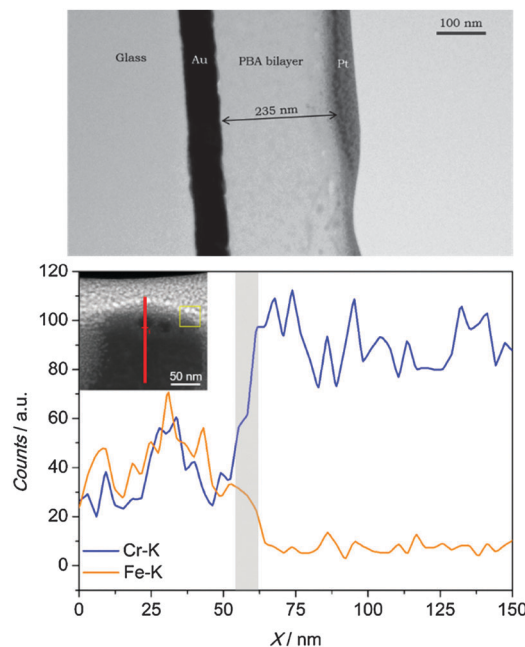


Fig. 2 Top: HR-TEM image of the lamella of the PBA bilayer. The Pt layer is added in order to protect the top surface of the bilayer from ion-beam induced damage during the HR-TEM lamella preparation. Bottom: STEM profile of the bilayer measuring the Fe content (orange curve) and Cr content (blue curve) in the system. The grey region indicates the interface between the two PBA layers. Inset: STEM image (scale: 50 nm) of the region under study in the lamella. The red line indicates the trace of the STEM profile and the yellow box is a cursor of the analysis program.

Finally, with the aim of having an alternative estimation of the thickness ratio between both PBAs composing the bilayer, chemical characterization by inductively coupled plasma mass spectrometry (ICP-MS) was performed. A bilayer was prepared, as previously described, on a Mylar substrate covered with gold. Subsequently, it was digested in a solution containing HNO$_3$ and HCl for its analysis. From the ICP analysis, relative amounts of 1536.3 mg kg$^{-1}$ of $^{52}$Cr and 300.2 mg kg$^{-1}$ of $^{56}$Fe are determined (see ESI,† for further details). Taking into account the stoichiometry of the compounds and different isotopic abundances, a ratio of 3 times more **CrCr** than **FeCr** in the bilayer is obtained. Since the density of the two layers is almost the same, this mass ratio can be translated into a volume ratio **CrCr**/**FeCr** = 3, which leads to a thickness of approximately 60 nm for the **FeCr** PBA film. This value matches the one expected from profilometry and STEM analyses. The agreement indicates a homogeneous covering of the two layers onto the electrode.

In summary, from a variety of characterization techniques it has been established that the thicknesses of the **CrCr** bottom layer and the **FeCr** top layer (both electrodeposited during 20 seconds) are, respectively, 175 nm and 60 nm. Clearly, there is a decrease of conductivity after deposition of the first layer and this translates into a slower kinetics of growth for the second top layer.

## Magnetic characterization

In the bilayer under study, the **CrCr** layer presents a ferrimagnetic behavior with an ordering temperature of 240 K, as previously

11124 | J. Mater. Chem. C, 2015, **3**, 11122–11128

This journal is © The Royal Society of Chemistry 2015

reported.[30,33] The hysteresis loop (Fig. S3, ESI†) of a 175 nm thick film of this material was measured at 2 K by SQUID magnetometry. From the maximum of the first derivative of the magnetization curve (inset Fig. S3a, ESI†), a coercive field of 60 Oe was obtained. The top **FeCr** is a ferromagnet with a critical temperature of 23 K.[35,36] A 60 nm thick film of this material shows a coercivity of 650 Oe (Fig. S3b, ESI†), obtained under the same conditions as those used for the **CrCr** film.

The characterization of the thermal dependence of the PBA bilayer by DC susceptibility was performed under field-cooled (FC) conditions in an external field of 100 Oe (Fig. 3). A first increase in susceptibility was observed at 240 K, corresponding to the ferrimagnetic ordering of the **CrCr** layer. Upon cooling below 23 K, a second transition was detected, being assigned to the Curie temperature of the **FeCr** layer. Thus, the presence of both intact PBAs in the bilayer is demonstrated from this measurement. No other transitions are observed from the FC characterization, indicating the absence of extra magnetic phases in addition to the electrodeposited materials.

The magnetic hysteresis loop obtained at 2 K for the PBA bilayer is shown in Fig. 4. The magnetic field was applied parallel to the surface, in the same way as that applied for the characterization of the isolated layers. Magnetization was then measured between +60 kOe and −60 kOe, but only the region with interesting magnetic information between +2 kOe and −2 kOe is shown.[38] The measurement, below the $T_c$ of both materials, exhibits two switching events that can be related to the reversal of each PBA in the mixed system. The parameter that will be treated in the discussion is the coercive field of each layer composing the structure. As it was done for the isolated PBA films, the coercivities in the bilayer were extracted from the derivative ($dM/dH$) of the first branch of the hysteresis. From this calculation a first coercive field of 115 Oe corresponding to the **CrCr** soft layer is determined. On the other hand, the second step related to the magnetization reversal process of the **FeCr** layer can be found at 1025 Oe, corresponding to the coercivity of this hard ferromagnetic layer. The coercive fields obtained in the PBA bilayer are clearly different and much higher than the values calculated for the isolated bottom and top layers, 60 Oe and 650 Oe, respectively. From these results it
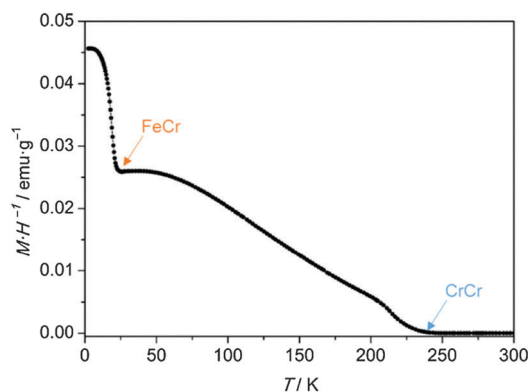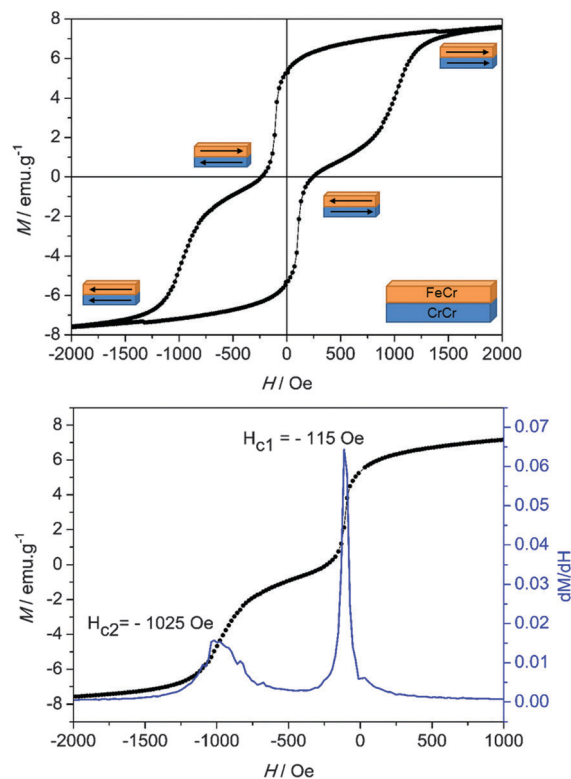


Fig. 4  Top: Hysteresis loop at 2 K of the PBA bilayer. Bottom: Derivative d$M$/d$H$ of the first branch of the hysteresis loop measured at 2 K for the PBA bilayer in direct contact, the coercive fields are Hc$_1$ = 115 Oe and Hc$_2$ = 1025 Oe.

is possible to infer that when both molecular-based magnetic materials are put in direct contact, magnetic coupling between both layers takes place.

These two requirements (soft and hard magnets in direct contact and the presence of an exchange coupling between them) are the ingredients to obtain exchange-spring magnets, ESM.[9,15,39,40] In these, the coupling between the two magnetic materials appears below a certain critical thickness of the soft layer, leading to a simultaneous magnetization reversal process.[14]

When this critical value is exceeded, a two-step feature appears in the hysteresis loop of the system,[14] just like in our situation. The first step is related to the formation of an ESM in the soft magnetic phase above a magnetic field denoted as a bending field[41] or a nucleation field, $H_N$. In this context, the soft layer is strongly pinned to the hard layer at the interface, meanwhile the outer region is free to follow the external magnetic field. Indeed, the dynamics of the spins in the soft layer resembles the one observed in a Bloch wall, with an increasing angle of rotation as the distance from the interface with the hard layer is increased. The second step in this hysteresis loop arises from the irreversible switching of the hard layer by progressively increasing the external magnetic field.

We can extend this scenario to understand the hysteresis loop features of our PBA bilayer (Fig. 4). Starting from a saturated situation in which the magnetization of both layers is in a parallel state, when the magnetic field reaches the value



Fig. 3  Thermal variation of the DC susceptibility ($M \cdot H^{-1}$) of the bilayer under FC conditions in an applied field of 100 Oe.

$H_N$, nucleation of the magnetization reversal of the softer **CrCr** layer takes place from the outer surface. Subsequently, the reversal process is extended through the whole **CrCr** phase until it is stopped by a potential barrier established by the presence of **FeCr** at the interface. Under these conditions, by increasing or decreasing the external magnetic field, the domain wall created in the soft layer can be compressed or decompressed, respectively, against the interface.[39,42]

In order to confirm the spring motion in the PBA bilayer, demagnetization curves in the region associated with the soft ferrimagnet reversal process were measured. Minor loops were registered for confirming the grade of reversibility of the magnetization reversal of the **CrCr** layer in the exchange spring process, as shown in Fig. 5. With this aim, the sample was poled up to +60 kOe, well above the saturation field of this material, after which minor loops between +300 Oe and −650 Oe were traced. It is important to remark that although the curve in Fig. 5 represents a minor loop for the overall bilayer system, it is actually a major loop for the **CrCr** ferrimagnetic layer.

Indeed, this curve is obtained by sweeping between extreme magnetic fields, which corresponds to the saturated states of **CrCr** magnetization (Fig. S3, ESI†). By performing this protocol, an "exchange-biased" loop is obtained for **CrCr** in the bilayer (Fig. 5), with a positive exchange bias field of $H_{EB}$ = 16.5 Oe calculated as[43]

$$H_{EB} = \frac{|H_{S+} + H_{S-}|}{2} \qquad (1)$$

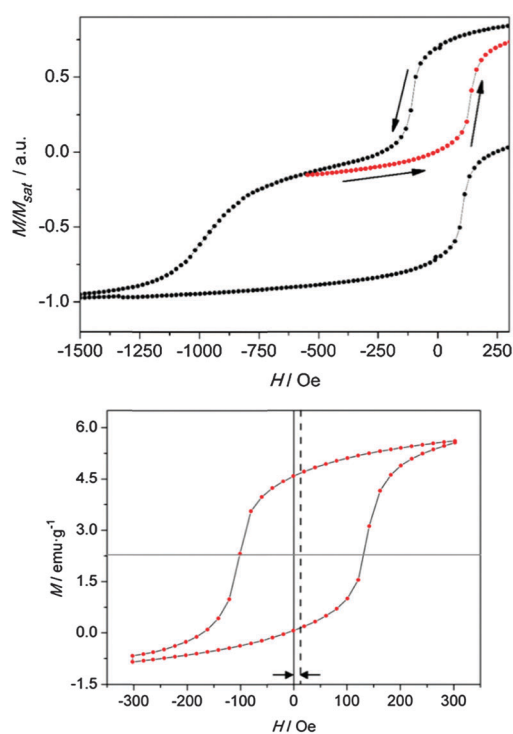According to this equation, the positive value of $H_{EB}$ agrees with the fact that the parallel orientation between Cr and Fe spins is preferred over the antiparallel arrangement. The small value of $H_{EB}$ could be associated with a non-epitaxial growth of the interfaces between both materials. Indeed, the exchange interactions in a bilayer are extremely affected by the defects and the interface quality, actually being more sensitive than any other structural probe.[44] In addition, a clear enhancement of the coercive field for this layer is detected with a value of $H_c$ = 115 Oe, being doubled with respect to the value corresponding to the isolated situation ($H_c$ = 60 Oe).

From all the presented information, it is possible to determine that the switching of the **CrCr** layer is reversible but hysteretic with respect to the exchange field $H_{EB}$ = 16.5 Oe, thus confirming in this sense the spring motion of the layer. In previous studies on ESMs composed by bilayers of SmCo/Co,[15] Fe/CoSm and Co/CoSm,[40] the hysteretic behavior of the minor loops, as the one observed in our system, was associated mainly with the strength of the magnetic anisotropy in the soft magnetic material. In our particular case, a possible anisotropy in the ferrimagnetic layer of **CrCr** can be discarded. From an ATR-IR study on thin films of this chromium cyanide PBA described elsewhere,[30] it was possible to detect a complete oxidation of $Cr^{2+}$ ions to $Cr^{3+}$ upon air exposure. The local anisotropy of the $Cr^{III}$ ions in the material can be neglected by considering the non-degenerate $^4A_{2g}$ ground state present in this metal ion. The isotropic character of the magnetic properties of **CrCr** was confirmed by SQUID measurements on films of this chromicyanide derivative with magnetic fields being applied parallel (longitudinal) and perpendicular to the surface (polar). This study showed unaltered values of the coercive field and magnetization for each configuration (Fig. S4, ESI†).[45] It has been shown that magnetic anisotropy in thin films can arise from demagnetization effects that are related to their two-dimensional nature.[46] However, this behaviour has been observed in samples prepared using a sequential adsorption method. In electropolymerization, the control of the relative orientation of the crystallites with respect to the substrate is poorer. Discarding the anisotropy of **CrCr**, the hysteretic behavior in the minor loop of the soft ferrimagnetic layer has to be associated with the other phenomenon. In this sense, the already mentioned weak interfacial exchange coupling strength, arising from the interface generated between these two polycrystalline materials,[14] has been proposed as a possible explanation.

The last point to treat is the effect of **CrCr** observed on the hard ferromagnetic layer. From Fig. 4 it is evident that the coercive field associated with the **FeCr** layer (1025 Oe) in the bilayer is clearly enhanced with respect to the isolated situation at the same temperature (650 Oe). For analyzing this result it is important to bear in mind that in the majority of the reported ESMs both materials are ferromagnetic, with only a few examples in which one or both layers are ferrimagnets.[42,47] When both layers are ferromagnets, a decrease of coercivity associated with the hard magnetic phase is observed. This can be explained by the propagation of the domain wall formed in the soft ferromagnet when it is compressed against the interface with the hard ferromagnet under an increasing magnetic field. This domain wall propagation initiates the magnetization reversal process at lower magnetic fields in the hard phase, reducing the coercive field of the material in this way.[15]
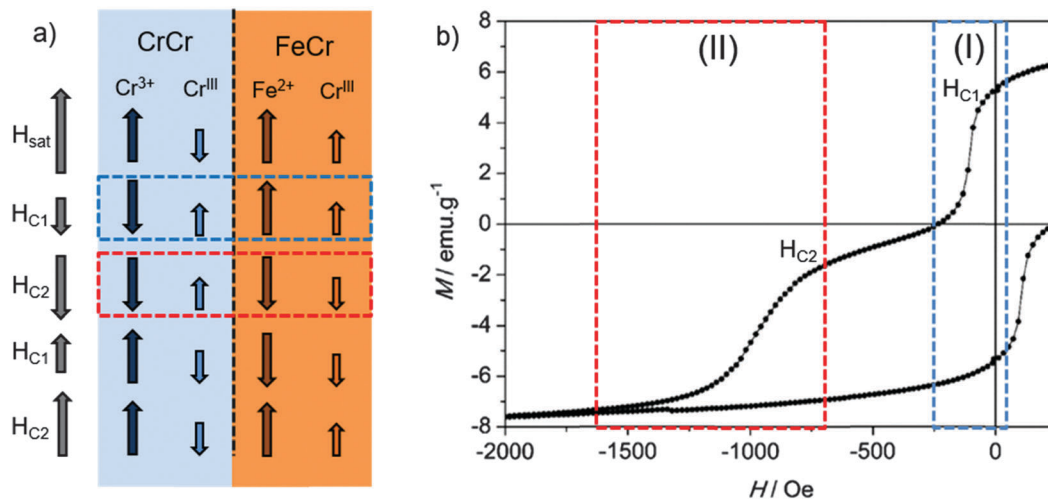


**Fig. 5** Top: Demagnetization curve at 2 K of the bilayer indicating the minor loop corresponding to the magnetization reversal process of the **CrCr** layer. Bottom: Exchange biased loop of the soft layer of **CrCr**.

Fig. 6 (a) Scheme of the spin configuration in each material according to the applied external magnetic field. $Cr^{III}$ and $Cr^{3+}$ correspond, respectively, to carbon-bonded and nitrogen-bonded chromium sites. Arrows are not local spins and simply denote the total magnetic moment of each sublattice. (b) Hysteresis loop of the bilayer measured at 2 K in which the regions corresponding to each reversal process of the layers are indicated. Region-I corresponds to the exchange-spring reversal process of the **CrCr** layer and region-II to the reversal of the **FeCr** layer.

In our molecule-based bilayer the effect observed on the hard ferromagnet is the opposite one. A possible explanation considers the nature of coupling at the interface. The ferrimagnetic **CrCr** film contains $Cr^{III}–C\equiv N–Cr^{3+}$ bridges giving rise to two magnetic sublattices of $S = 3/2$ spins. Since there are approximately two $Cr^{III}$ centers per three $Cr^{3+}$ ions, the spins do not compensate and a net magnetic moment appears. At saturating fields, the $Cr^{III}$ sublattice is thus antiparallel to the magnetic field, whereas the $Cr^{3+}$ sublattice is parallel (Fig. 6). The **FeCr** film consists of $Cr^{III}–C\equiv N–Fe^{2+}$ bridges. The $Cr^{III}$ ($S = 3/2$) and $Fe^{2+}$ ($S = 2$) spins are aligned parallel to the magnetic field, as expected for a ferromagnetic material.

At the interface, the relative orientation of the $Cr^{III}$ and $Fe^{2+}$ magnetic moments depends on the value of the applied field. At saturating fields, it is antiparallel (Fig. 6a). In region I (blue box in Fig. 6a and b), a parallel arrangement of the spins is expected. Finally, in region II (red box in Fig. 6a and b), the relative arrangement of $Cr^{III}$ ($S = 3/2$) and $Fe^{2+}$ ($S = 2$) spins is again antiparallel.

Still, this antiparallel orientation is unfavoured since the coupling for this pair of centres is expected to be ferromagnetic and, furthermore, the $Fe^{2+}$ ions have a large magnetic anisotropy. Thus, at fields sufficiently large for switching the **CrCr** layer, the exchange field at the interface dominates the reversal of the **FeCr** hard layer. This process leads to an enhancement of the value of **FeCr** coercivity with respect to the isolated case.

## 4. Conclusions

In the present work the possibility of fabricating a bilayer of PBA magnetic thin films at the nanometer level has been demonstrated. This bilayer exhibits a magnetic coupling between the two components. Extra characterization, such as polarized neutron reflectivity, should be performed in the bilayer in order to confirm the nature

of the exchange coupling existing between the two materials, as well as to obtain a complete description of the domain wall formation process. The fabrication of this structure has been achieved by means of a solution process method. Thin films of these molecular-based materials have been electropolymerized by a sequential coulometric procedure. By using this method we have been able to put a soft ferrimagnetic layer of the **CrCr** PBA in direct contact with a hard ferromagnetic layer formed by a **FeCr** layer, allowing the detection of an exchange-spring magnet behavior in an all molecular-based system.

## Acknowledgements

## Notes and references

1  C. P. Meiklejohn and W. H. Bean, *Phys. Rev. Lett.*, 1957, **105**, 904–913.
2  J. Nogués and I. K. Schuller, *J. Magn. Magn. Mater.*, 1999, **192**, 203–232.
3  J. Nogués, J. Sort, V. Langlais, V. Skumryev, S. Suriñach, J. S. Muñoz and M. D. Baró, *Phys. Rep.*, 2005, **422**, 65–117.
4  R. L. Stamps, *J. Phys. D: Appl. Phys.*, 2001, **34**, 444.
5  V. Fontaiña-Troitiño, N. Rivas-Murias, B. Rodriguez-Gonzalez and B. Salgueiriño, *Chem. Mater.*, 2014, **26**, 5566–5575.
6  J. Camarero, J. Sort, A. Hoffmann, J. García-Martín, B. Dieny, R. Miranda and J. Nogués, *Phys. Rev. Lett.*, 2005, **95**, 057204.

7  E. F. Kneller and R. Hawig, *IEEE Trans. Magn.*, 1991, **27**, 3588–3600.

8  J. S. Jiang, E. E. Fullerton, M. Grimsditch, C. H. Sowers and S. D. Bader, *Phys. Rev. B: Condens. Matter Mater. Phys.*, 1998, **58**, 193–200.

9  E. E. Fullerton, J. S. Jiang and S. D. Bader, *J. Magn. Magn. Mater.*, 1999, **200**, 392–404.

10  H. Zeng, J. Li, J. P. Liu, Z. L. Wang and S. Sun, *Nature*, 2002, **420**, 395–398.

11  R. Kiwi, M. Mejía-López, J. Portugal and R. D. Ramírez, *Europhys. Lett.*, 1999, **48**, 573–579.

12  R. Skomski and J. M. D. Coey, *Phys. Rev. B: Condens. Matter Mater. Phys.*, 1993, **48**, 15812–15816.

13  T. Schrefl, H. Kronmüller and J. Fidler, *J. Magn. Magn. Mater.*, 1993, **127**, L273–L277.

14  G. H. Guo, G. F. Zhang and X. G. Wang, *J. Appl. Phys.*, 2010, **108**, 043919.

15  E. E. Fullerton, J. S. Jiang, C. H. Sowers, J. E. Pearson and S. D. Bader, *Appl. Phys. Lett.*, 1998, **72**, 380–382.

16  L. Catala, D. Brinzei, Y. Prado, A. Gloter, O. Stéphan, G. Rogez and T. Mallah, *Angew. Chem., Int. Ed.*, 2009, **48**, 183–187.

17  Y. Prado, N. Dia, L. Lisnard, G. Rogez, F. Brisset, L. Catala and T. Mallah, *Chem. Commun.*, 2012, **48**, 11455.

18  M. Clemente-León, E. Coronado, C. J. Gómez-García, M. López-Jordà, A. Camón, A. Repollés and F. Luis, *Chem. – Eur. J.*, 2014, **20**, 1669–1676.

19  S. I. Ohkoshi and K. Hashimoto, *J. Am. Chem. Soc.*, 1999, **121**, 10591–10597.

20  K. Sato, O. Iyoda, T. Fujishima and A. Hashimoto, *Science*, 1996, **272**, 704–705.

21  M. Escax, V. Bleuzen, A. Cartier dit Moulin, C. Villain, F. Goujon, A. Varret and F. Verdaguer, *J. Am. Chem. Soc.*, 2001, **123**, 12536–12543.

22  S. Margadonna, K. Prassides and A. N. Fitch, *Angew. Chem., Int. Ed.*, 2004, **43**, 6316–6319.

23  E. Coronado, M. C. Giménez-López, G. Levchenko, F. M. Romero, V. García-Baonza, A. Milner and M. Paz-Pasternak, *J. Am. Chem. Soc.*, 2005, **127**, 4580–4581.

24  E. Coronado, M. C. Giménez-López, G. Levchenko, F. M. Romero, A. Segura, J. C. Cezar, F. M. F. De Groot, A. Milner and M. Paz-pasternak, *J. Am. Chem. Soc.*, 2008, **130**, 15519–15532.

25  S. I. Ohkoshi, H. Tokoro and K. Hashimoto, *Coord. Chem. Rev.*, 2005, **249**, 1830–1840.

26  D. M. Pajerowski, M. J. Andrus, J. E. Gardner, E. S. Knowles, M. W. Melsel and D. R. Talham, *J. Am. Chem. Soc.*, 2010, **132**, 4058–4059.

27  M. F. Dumont, E. S. Knowles, A. Guiet, D. M. Pajerowski, A. Gomez, S. W. Kycia, M. W. Meisel and D. R. Talham, *Inorg. Chem.*, 2011, **50**, 4295–4300.

28  M. F. Dumont, E. S. Knowles, A. Guiet, D. M. Pajerowski, A. Gomez, S. W. Kycia, M. W. Meisel and D. R. Talham, *Inorg. Chem.*, 2011, **50**, 4295–4300.

29  C. R. Gros, M. K. Peprah, B. D. Hosterman, T. V Brinzari, P. A. Quintero, M. Sendova, M. W. Meisel and D. R. Talham, *J. Am. Chem. Soc.*, 2014, **136**, 9846–9849.

30  E. Coronado, M. Makarewicz, J. P. Prieto-Ruiz, H. Prima-Garcia and F. M. Romero, *Adv. Mater.*, 2011, **23**, 4323–4326.

31  H. Prima-Garcia, E. Coronado, J. P. Prieto-Ruiz and F. M. Romero, *Nanoscale Res. Lett.*, 2012, **7**, 232.

32  T. Mallah, S. Thiébaut, M. Verdaguer and P. Veillet, *Science*, 1993, **262**, 1554–1557.

33  K. Sato, O. Iyoda, T. Fujishima and A. Hashimoto, *Science*, 1996, **271**, 49–51.

34  W. E. Buschmann, S. C. Paulson, C. M. Wynn, M. A. Girtu, A. J. Epstein, H. S. White and J. S. Miller, *Chem. Mater.*, 1998, **4756**, 1386–1395.

35  E. Coronado, M. Fitta, J. P. Prieto-Ruiz, H. Prima-García, F. M. Romero and A. Cros, *J. Mater. Chem. C*, 2013, **1**, 6981–6988.

36  S. Ohkoshi, Y. Einaga, A. Fujishima and K. Hashimoto, *J. Electroanal. Chem.*, 1999, **473**, 245–249.

37  J. A. Nakanishi, S. Lu, G. Kothari, H. M. Bohannan and E. W. Switzer, *J. Am. Chem. Soc.*, 2003, **125**, 14998–14999.

38  The magnetization at the highest field of the experiment (5 T) equals 1. 33 $\mu_B$, far from saturation and even much lower than the expected value for isolated **CrCr** films (4.5 $\mu_B$). Deviations between the expected and reported values of magnetization at saturation are the rule for **FeCr** and **CrCr** (both as powders and films), and are normally ascribed to a combination of anisotropy factors and structural disorder that leads to a spin-glass behaviour.

39  F. Canet, C. Bellouard, L. Joly and S. Mangin, *Phys. Rev. B: Condens. Matter Mater. Phys.*, 2004, **69**, 1–11.

40  T. Nagahama, K. Mibu and T. Shinjo, *J. Phys. D: Appl. Phys.*, 1999, **31**, 43–49.

41  E. Goto, N. Hayashi, T. Miyashita and K. Nakagawa, *J. Appl. Phys.*, 1965, **36**, 2951–2958.

42  A. V. Ramos, J. B. Moussy, M. J. Guittet, M. Gautier-Soyer, C. Gatel, P. Bayle-Guillemaud, B. Warot-Fonrose and E. Snoeck, *Phys. Rev. B: Condens. Matter Mater. Phys.*, 2007, **75**, 1–8.

43  K. Ziese, M. Höhne, R. Bollero, A. Semmelhack, H. C. Esquinazi and P. Zimmer, *Eur. Phys. J. B*, 2005, **45**, 223–230.

44  R. J. Suzuki, Y. van Dover, R. B. Gyorgy, E. M. Phillips and J. M. Felder, *Phys. Rev. B: Condens. Matter Mater. Phys.*, 2006, **53**, 14016–14019.

45  E. Coronado, J. P. Prieto-Ruiz and H. Prima-Garcia, *Chem. Commun.*, 2013, **49**, 10145–10147.

46  D. M. Pajerowski, J. E. Gardner, M. J. Andrus, S. Datta, A. Gomez, S. W. Kycia, S. Hill, D. R. Talham and M. W. Meisel, *Phys. Rev. B: Condens. Matter Mater. Phys.*, 2010, **82**, 1–5.

47  M. B. Demirtas, S. Hossu, M. R. Arikan, M. Koymen and A. R. Salamon, *Phys. Rev. B: Condens. Matter Mater. Phys.*, 2007, **76**, 1–7.

11128 | *J. Mater. Chem. C*, 2015, **3**, 11122–11128

This journal is © The Royal Society of Chemistry 2015